Rizatriptan benzoate-loaded dissolving microneedle patch for management of acute migraine therapy

Abstract: In this study, dissolving microneedles (MNs) using polyvinyl alcohol (PVA) and poly(1-vinylpyrrolidone-co-vinyl acetate) (P(VP-co-VA)) as matrix materials were developed for transdermal delivery of rizatriptan benzoate (RB) for acute migraine treatment. *In-vitro* permeation studies were conducted to assess the feasibility of the as-fabricated dissolving MNs to release RB. Drug skin penetration were tested by Franz diffusion cells, showing an increase of the transdermal flux compared to passive diffusion due to the as-fabricated dissolving MNs having a sufficient mechanical strength to penetrate the skin and form microchannels. The pharmacological study *in vivo* showed that RB-loaded dissolving MNs significantly alleviated migraine-related response by up-regulating the level of 5-hydroxytryptamine (5-HT) and down-regulating the levels of calcitonin gene-related peptide (CGRP) and substance P (SP). In conclusion, the RB-loaded dissolving MNs have advantages of safety, convenience, and high efficacy over conventional administrations, laying a foundation for the transdermal drug delivery system treatment for acute migraine.

Keywords: Microneedles, migraine, rizatriptan benzoate, transdermal drug delivery

1. Introduction

Migraine is a prevalent neurovascular disorder that affects more than one billion people worldwide [1]. It manifests as recurrent and often unilateral headache attacks, accompanied by photophobia, phonophobia, nausea and vomiting [2]. Among the various mechanisms, activation of the trigeminal vascular system is considered to be the core of migraine pathophysiology [3, 4]. CGRP is released from trigeminal nerve C-fibers upon stimulation by sensory neurons in the trigeminal ganglion. CGRP is a potent vasodilatory neuropeptide that acts on the middle meningeal artery to induce cranial vasodilation and stimulate Aδ-fibers expressing calcitonin receptor-like receptor/receptor activity-modifying protein ($CLR/RAMP_1$, CGRP receptor) [5]. CGRP receptor activation, which in turn initiates adenylate cyclase (AC) activation, causes the accumulation of intracellular cyclic adenosine monophosphate (cAMP), cAMP-dependent sensitization of Aδ-fibers and enhanced nociceptive transmission in the trigeminal caudate nucleus [6, 7].

One of the current targets for migraine treatment is the 5-HT receptor [8, 9]. The $5\text{-}HT_{1B}$ receptor ($5\text{-}HT_{1BR}$) is a Gi-coupled receptor that is an important target for treating 5-HT neurotransmission-related diseases such as migraine, depression and anxiety. When triptan drugs act as 5-HT receptor agonists and bind to $5\text{-}HT_{1B/1D}$ receptors coupled with Gi proteins, they cause a decrease of cAMP levels in cells, resulting in a reduction of CGRP released from trigeminal nerve cells, ultimately reducing nociceptive transmission [10-12].

5-HT receptor agonists mainly relieve migraine attacks by activating $5\text{-}HT_{1A/B/D}$

receptors, causing vasoconstriction and lowering cAMP levels when acting on 5-HT_{1B} receptors, inhibiting CGRP release from C-fibers through voltage-gated calcium channels [13, 14]. Triptan-based drugs act as 5-$HT_{1B/1D}$ receptor agonists and have been used as the first choice specific drugs for acute treatment of migraine [15], and it significantly inhibit CGRP release from trigeminal nerve terminals by binding and activating presynaptic 5-HT_{1D} and 5-HT_{1F} receptors [16]. Due to its peripheral vasodilatory effect, it is contraindicated in patients with cardiovascular diseases, uncontrolled hypertension, or hemiplegic migraine with complex aura [17]. Substance P (SP), a neuropeptide discovered in 1931 in the intestines and brains of horses, has the ability to cause smooth muscle contraction, vasodilation, and blood pressure reduction. It is widely distributed in central and peripheral nervous tissues and can transmit pain and lower pain thresholds. Trigeminal nerve innervation releases vasoactive neuropeptides such as CGRP and SP, which play a core role in neurogenic inflammation in migraine [18, 19]. C-fos, as a constituent of the proto-oncogene fos family (comprising c-fos, fosB, fra-1 and fra-2), is an immediate early gene and an indicator of neuronal activity. When subjected to some noxious stimuli, such as intense light, mechanical damage, chemical injury, etc., the expression of c-fos in neurons is significantly increased. It can be utilized to delineate the regions of neuronal activation in pain research, and has been extensively applied in the investigations of migraine pathophysiology and efficacy [20, 21].

RB is a second-generation triptan that offers rapid headache relief with fewer adverse effects than the other triptans [22]. It is also a primary pharmacological agent

for migraine management. After oral administration, RB reaches its peak plasma concentration within 1 to 1.5 h. However, its oral bioavailability is limited by hepatic first-pass metabolism and low absorption efficiency, resulting in an average oral bioavailability of only 45 % [23]. Moreover, subcutaneous (S.C.) injections are poorly tolerated by patients. RB orally disintegrating tablets can increase the bioavailability of RB, shorten its onset time, and reduce its degradation and metabolism in the gastrointestinal tract [24], but the disadvantage of this route is that it may cause oral discomfort, such as burning sensation, numbness, bitterness, etc. [25]. Nasal and oral inhalation are the new route of administration, and RB nasal spray has been developed in clinical practice in recent years [26]. Although triptan nasal sprays have good efficacy and fast onset, nasal formulations still face some challenges [27]. Due to the presence of ciliary movement and mucosal absorption barrier, it is an obstacle to obtain effective drug absorption through the nasal route [28]. To overcome the drawbacks of oral and injectable routes, transdermal drug delivery has emerged as a promising modality in the therapeutic industry, offering advantages such as high bioavailability, enhanced compliance, reduced dosing frequency, and painlessness [29, 30].

MNs are needle-like structure with a height of 10-2,000 μm and a width of 10-50 μm, which can pierce the epidermal layer and reach the dermal tissue without causing pain [31]. Therefore, MNs are the ideal choice for enhancing patient adherence as they avoid stimulating the pain-sensitive nerves [32]. In recent years, MNs have been used to deliver various therapeutic agents, such as drugs, genes, proteins, RNA, and vaccines, and have demonstrated remarkable therapeutic effects [33, 34]. One of the most

important applications for which MNs have great potential is vaccine delivery [35]. MNs can overcome the limitations of conventional vaccine delivery methods by delivering vaccines into the skin, which is rich in antigen-presenting cells and immune cells. MNs also can enhance the immunogenicity and efficacy of vaccines by targeting specific skin layers or cells [36, 37]. Another important application of MNs is combination drug delivery to treat complex diseases that require multiple drugs, such as cancer, diabetes, arthritis, obesity, neurological diseases and glaucoma. In short, MNs can provide a convenient and effective platform for combination drug delivery by incorporating different drugs into different parts or types of MNs [38, 39]. For acute migraine therapy, a portable treatment that can rapidly alleviate headaches and eliminate the associated symptoms would be desirable [40, 41].

Dissolving MNs are a painless, minimally invasive, and self-administered transdermal delivery system with high drug bioavailability [42]. They offer advantages over syringes in terms of patient compliance and adverse reactions. Moreover, dissolving MNs have the features of rapid dissolution and short application time, which can reduce the delivery time and enhance the delivery efficiency [43]. It is usually required to be taken as soon as possible during a migraine attack to achieve the optimal effect [44]. Therefore, using dissolving MNs as a RB delivery platform can provide fast, effective, safe and convenient treatment. PVA is a water-soluble polymer with good biocompatibility and low toxicity, which has been widely used in biomedical systems [45, 46]. P(VP-co-VA) has excellent adhesion and biocompatibility, low hygroscopicity, and easy storage as a MNs material [47]. However, it has high brittleness and is difficult

to insert into the skin when used as MNs matrix alone. By combining with PVA, the toughness and mechanical strength of MNs can be improved synergistically.

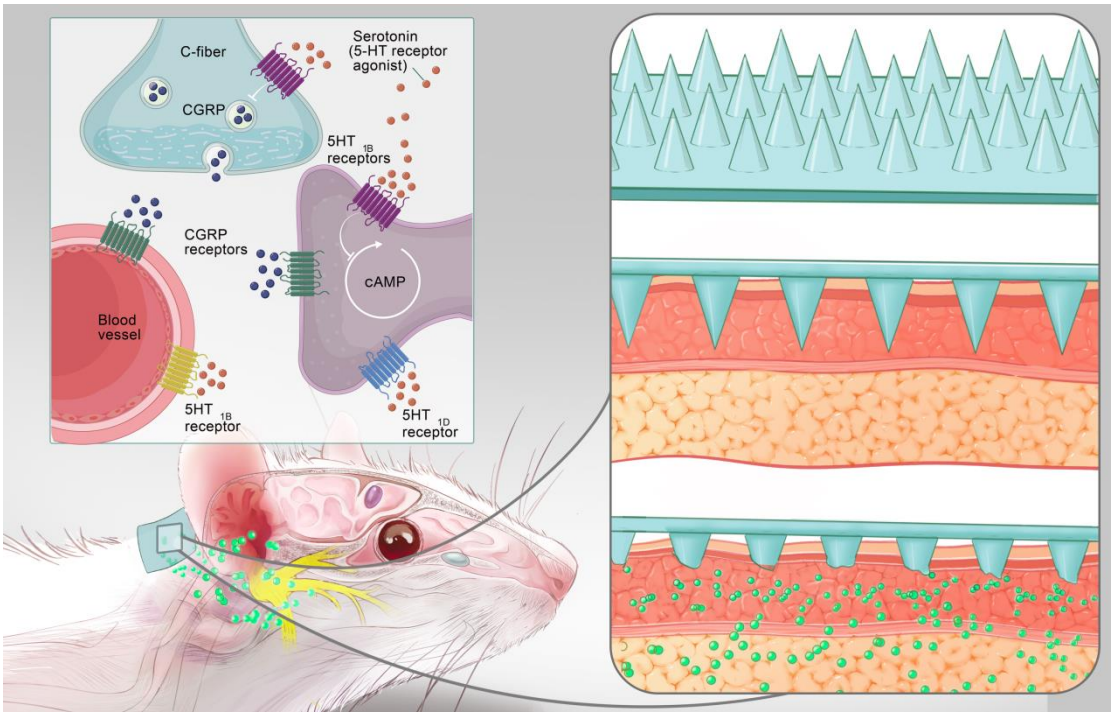

Fig. 1 Schemetic illustration of RB-loaded MNs for acute migraine treatment.

Based on the above considerations, we developed rapidly dissolving MNs derived from biodegradable materials. This study aimed to develop RB-loaded MNs for acute migraine therapy. RB-loaded MNs were fabricated by the micro-molding technique. P(VP-co-VA) and PVA with excellent biocompatibility and biodegradability, were chosen as the matrix materials for fabrication of dissolving MNs. RB was incorporated into the MNs matrix, and the morphology, size, and mechanical properties of the as-fabricated MNs were evaluated as well. Upon insertion into the skin, the matrix at the tip of the MNs dissolved rapidly, enabling the fast release and diffusion of RB into deeper skin layers through the microchannels created by the MNs (Fig. 1) [48-50].

2. Materials and methods

2.1 Materials

Poly(vinyl alcohol) (PVA, Mw = ~150,000) and poly(1-vinylpyrrolidone-co-vinyl acetate) (P(VP-co-VA), Mw = ~13,000) were purchased from Aladdin (Shanghai China). Rizatriptan benzoate and gelatin were purchased from Macklin (Shanghai China). Phosphate-buffered solution (PBS) and Rhodamine B (RhB) were obtained from Rhawn (Shanghai, China). 5-HT, CGRP and SP ELISA Kits were obtained from Elabscience Biotechnology Co., Ltd. (Wuhan, China). C-fos antibody was purchased from Bioss Biotechnology Co., Ltd. (Beijing, China). Nitroglycerin injection was purchased from Guangzhou Pharmaceutical Holdings Limited (Guangzhou, China).

2.2 Fabrication of MNs

The negative mold of the 39×39 MNs (800 μm height and 200 μm base) array in polydimethylsiloxane (PDMS) were obtained from Lake Mould Co., LTD (Suzhou, China). PVA and P(VP-co-VA) were dissolved in deionized water (DI) to prepare 15% w/v solutions and then mixed at a 1:1, 2:1 and 1:2 volume ratio to obtain a blended solution, which served as a precursor solution to prepare backing layer of the MNs. Although RB is a hydrophobic drug with low solubility in water (32.9 ± 0.2 mg/mL) [26]. To fabricate RB-loaded dissolving MNs, 10 mg of RB was mixed with the 20 mL of PVA/P(VP-co-VA) blended solution. Then, the mixture of RB and polymers was stirred at room temperature for 2 h to ensure the homogeneity of the drug in the polymer solution to form 0.05% w/v drug-loaded solution for fabrication of MNs tips. PVA, P(VP-co-VA) and PVA/P(VP-co-VA) MNs were cast by centrifugal molding and a double-layer casting process was employed to fabricate the RB-loaded MNs. The RB and PVA/P(VP-co-VA) blended solution was firstly costed on MNs molds, and removed

the excess solution after filling the cavities of the MNs mold through centrifugation method with 1,000 rpm for 2 h at 30°C. Then, PVA/P(VP-co-VA) blended solution was spread on the MNs mold to form the backing patch of MNs. The filled molds were dried in an oven at 37°C for 24 h, and the RB-loaded MNs could be obtained after carefully peeling off from the molds. The dose of RB in each MNs was ~ 0.5 mg that determined by the previous methods [51, 52]. The drug-free MNs were also obtained by the same procedure.

2.3 Characterization of matrix of MNs

FTIR spectra were performed in Fourier infrared spectrometer (Nicoet170SX, Nicoet Company, USA) using potassium bromide tablet method with wavenumber range of 500-4,000 cm^{-1}. Thermal characterization of RB, PVP/P(VP-co-VA) and RB/PVA/P(VP-co-VA) was studied by a DSC machine (TA Instruments, Surrey, UK). The sample masses were in the range of 2-3 mg, and scanning temperature rate was 10 °C/min from 25 to 300 °C. The heat flow signals were recorded as a function of temperature. All DSC tests were performed under a nitrogen flow rate of 20 mL/min.

2.4 Mechanical property test

The mechanical performance of RB-loaded MNs was assessed by a universal material testing machine (WDW-02, Tian Chen Testing Machine Co. LTD., Jinan, China). MNs were placed on a flat rigid surface of a stainless steel substrate. A moving sensor perpendicular to the MNs axis applied an axial force at a constant speed of 18 mm/min. The initial distance from the tip of the MNs to the holder was set at 1 cm. The force was recorded as the motion sensor touched the uppermost end of the MNs. The

test machine then recorded the force required to move the holder as a function of MNs displacement and plotted the displacement-force diagram [53, 54].

To evaluate the skin penetration and diffusion ability of MNs *in vivo*, RhB-loaded MNs prepared by the same fabrication process using Rhodamine B (RhB) as model drug. And they were inserted into the excised porcine skin using the finger pressing method for 5 min to ensure all MNs tips. After removing the MNs from the surface of skin, the skin was rinsed with DI water to ensure no residual red dye on the skin surface. The penetration situation of the MNs was observed under a digital microscope (Emspira 2, Leica, Wetzlar, Germany). To assess their toughness, MNs were evaluated by the static pressure tests against 100, 200 and 500 g weights for 20 min on the tips of them, and the bending shape of MNs tips were recorded by an optical microscope.

2.5 *In vitro* drug permeation study

The Franz diffusion cells was used to assess the drug release across the skin. The skin of rats was secured between the supply and receiver pools and thawed on the bench with the stratum corneum facing upward. The receiving cell was filled with PBS (pH = 7.4) and stirred at 37°C [55]. The RB-loaded MNs were gently inserted into the skin surface using an uniform pressure to ensure all MNs tips inserted into skin tissue. At predetermined time intervals, 1 mL of 0.1 $mol \cdot L^{-1}$ PBS solution was taken out to measure the concentration of RB in the solution. Meanwhile, 1 mL fresh PBS was added into receiving cell to keep the unchanged of in the diffusion conditions. The RB-loaded MNs were further soaked in 20 mL of PBS solution to determine the dose of RB in the MNs. The extracted PBS samples were analyzed by UV spectrophotometer (TU-1901,

Purkinje General Instrument Co., Ltd., Beijing, China) using a pre-set standard curve of rizatriptan benzoate at 280 nm (Fig. S1).

2.6 Skin penetration tests *in vitro*

The dye was loaded into the MNs by dissolving of RhB in the polymer solution before coating on the mold, and then pressed onto stretched rat skin tissues with a force of 30 N for 5 min before removing of them. The skin was embedded and frozen in an O.C.T. compound, which was cut into 10 μm thickness sections for histological observation and drug diffusion by a confocal laser scanning microscope (CLSM, C2, Nikon Corporation, Japan).

2.7 Pharmacological study *in vivo*

The rats were provided with unrestricted water and food for 12 h under a light-dark cycle and acclimated for 3 days. The rats were randomly divided into five groups, namely control group (no migraine induction and no treatment), blank group (treatment by oral saline), subcutaneous injection group (subcutaneous injection of RB solution ~0.5 mg/pcs through abdominal skin), oral administration group (oral gavage of RB solution ~0.5 mg/pcs) and the RB-MNs group (treatment by RB-loaded MNs on abdominal skin). The migraine rat model was established by subcutaneous injection of 1 mg/mL of nitroglycerin (NTG) into the neck except for the blank group [56, 57]. The behavioral alterations of the rats, such as cage climbing and head-scratching, were recorded at 0-30, 30-60, 60-90, 90-120, 120-180 and 180-240 min after drug administration. Blood samples (250 μL) were collected from the jugular vein catheter using gel separator tubes containing lithium heparin at 5, 15, 30, 60, 90, 120, 180, and

240 min after administration. All blood samples were centrifuged at 3000 r/min at 4℃ for 10 min to obtain plasma, and the extracted samples were analyzed by HPLC using a pre-set standard curve of rizatriptan benzoate at 280 nm (Fig. S2). The levels of 5-HT, CGRP, and SP in blood samples at 120 and 240 min were assessed by an enzyme-linked immunoassay kit. All animal studies were approved by the Experimental Animal Ethics Committee of the Eyoung Pharmaceutical Research and Development Centre of Zhejiang Province and Zhejiang Sci-Tech University Laboratory Animal Ethics Committee (Number: ZJEY-20221128-04). All experiments followed the instructions of the Laboratory Animal Care and Use Guide.

2.8 Partial immunohistochemistry of brain stem

The rat's head hair was cut off with medical scissors 4 h after drug administration, the skin was removed and disinfected with 75% medical alcohol. The scalp was incised to expose the occipital bone, which was partially removed with small medical biting forceps through the large hole. After full exposure of the brain tissue and discarding the dura mater, the brain stem was separated from the cerebral hemisphere and fixed in 4% paraformaldehyde solution. Immunohistochemistry was performed to determine the c-fos protein expression in the brain tissue.

2.9. Statistical analysis

SPSS 25 statistical software was used to analyze the data, and the data of each group were first judged to determine whether they conformed to a normal distribution and the chi-square test. If they conformed to normal distribution and chi-square, then the data were expressed as mean ± standard deviation, all using the method of one-way

ANOVA with LDS test. If they did not conform to normal distribution and chi-square, the comparison between the groups was fabricated by non-parametric test. Differences were considered statistically significant at *P < 0.05 and **P<0.001.

3. Results and discussion

3.1 Fabrication and characterization of RB-loaded MNs

The RB-loaded MNs were fabricated by a micro-molding technique using P(VP-co-VA) and PVA as the matrix materials. RB was incorporated into the MNs matrix, After drying in an oven at 37°C for 24 h, the MNs with 39 × 39 array on a patch could be obtained (Fig. S3). Fig. 2a and 2b display the digital microscopic images of the MNs, indicating a regular microneedle arrays. The prepared MNs had a pyramid-shape with height about 800 μm and width ~ 200 μm, respectively. The width of the adjacent substrate of the MNs were about 300 μm (Fig. 2c and 2d).

FT-IR was used to assess the possible physio-chemical interactions between RB and matrix (P(VP-co-VA) and PVA) in the MNs. As shown in Fig. 2e, the characteristic peaks of RB are observed at 1,606 and 1,506 cm^{-1}, ascribing to the C=C stretching vibration of the aromatic ring. The peak at 1,566 cm^{-1} can be contributed to the C-N stretching vibration. And the peaks at 887 and 724 cm^{-1} are originated from the C-H out-of-plane bending vibration of the aromatic ring [58]. For the native PVA and P(VP-co-VA), the characteristic peak of P(VP-co-VA) block polymer is 1,724 cm^{-1}, indicating the presence of the C=O groups. The typical broad peak around 3,300 cm^{-1} is ascribed to hydroxyl group (O-H) stretching [59]. In RB-loaded MNs, all typical peaks of RB and MNs matrix can be observed, showing that RB is physically

encapsulated in the MNs. The DSC curves of RB, blank, and RB-loaded MNs are shown in Fig. 2f. The melting point of native RB is 181.2 °C, suggesting its crystalline nature [26]. As an amorphous biopolymer, P(VP-co-VA) and PVA have no melting point below 200 °C. The PVA is a semicrystalline polymer with melting temperature around 220 °C. In the case of RB-loaded MNs, the typical melting point of RB and PVA with slight and negligible differences can be observed, further indicating that the RB is physically dispersed in the matrix [60, 61].

One of the main criteria for polymer MNs is to have sufficient mechanical strength to penetrate the skin. The mechanical properties of the fabricated MNs with different compositions are tested using a universal material testing machine. The force-displacement curves of RB-loaded and drug-free MNs based on PVA/P(VP-co-VA) show no abrupt changes within 0-300 μm. After displacement more than 300 μm, the forces show a rapid increased, but no fracture occurred, indicating the excellent toughness of MNs. At a displacement of 600 μm, the maximum forces for RB-loaded and drug-free MNs (1:1) are 1.93 and 1.75 N/needle, compared with blank MNs with PVA/P(VP-co-VA) = 2:1 and 1:2 which are 1.63 and 1.60 N/needle, respectively. The mechanical properties of MNs formed by PVA and P(VP-co-VA) alone are 1.32 and 0.16 N/needle, which are inferior to those formed by mixed matrix. However, a fracture at 300 μm is observed in case of MNs fabricated by P(VP-co-VA), indicating the poor toughness and mechanical strength (Fig. 2g). Therefore, the blend of PVA and P(VP-co-VA) (1:1) are chosen as the matrix of MNs for the following research due to their excellent biodegradability, biocompatibility, and rapid metabolism and excretion [45,

46, 50]. In addition, the MNs are further evaluated by a static pressure test. As shown in Fig. 2h, no broken MNs can be founded even pressed by 500 g weights for 20 min, indicating the excellent toughness and mechanical strength of as-fabricated MNs.

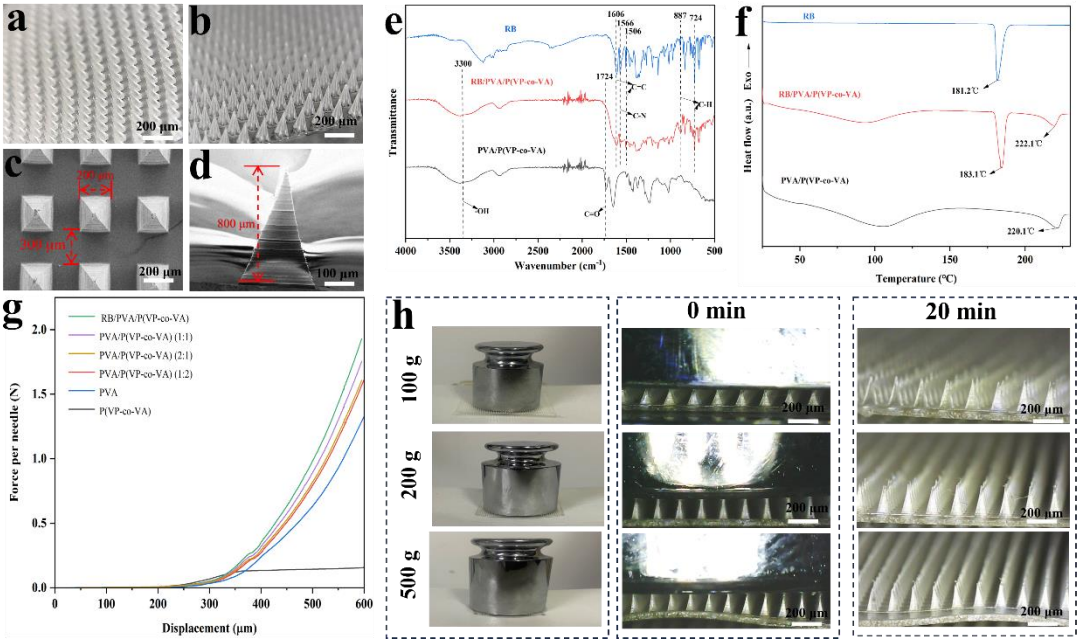

Fig. 2 The morphology and mechanical performance of the as-fabricated MNs. Bright-field microscopy image of MNs (a and b). SEM images of MNs (c, top view) and corresponding high magnification area of a single needle (d). (e) FT-IR spectra of RB, RB/PVA/P(VP-co-VA) and PVA/P(VP-co-VA) (f) DSC results of RB, RB/PVA/P(VP-co-VA) and P(VP-co-VA). (g) Mechanics-displacement curves of PVA, P(VP-co-VA), RB-loaded MNs and blank MNs. (h) Morphology changes of MNs before and after static pressure tests.

3.2 Drug release and insertion tests of MNs

The Franz diffusion cells is used to assess the drug release across the skin. Fig. 3a shows the release profile of RB-loaded MNs *in vitro*, a rapid release can be observed in the first 60 min, which may be the diffusion of RB through the microchannels that form by MNs, resulting in a faster initial release close to 75%. Further increasing the drug release time to 2 h, more than 95% RB can be diffused into receiving cells. Then, the as-fabricated RB-loaded MNs are further soaked in PBS solution to determine the content of RB in the MNs. The dose of RB in RB- MNs is ~ 0.502 ± 0.006 mg/patch

that calculate by the standard curve of RB in the solution (Table S1). To investigate the insertion of MNs, RhB-loaded MNs are prepared using the same method. Fig. 3b shows the digital image of RhB-loaded MNs that dyed by red color. The prepared RhB-loaded MNs are used for skin insertion test. The RhB-loaded MNs are inserted into porcine cadaver skin after applying a constant force. And the MNs are removed after 2 min, a series of red dots corresponding to the insertion sites of the MNs can be displayed on the skin surface (Fig. 3c and 3d). The as-fabricated MNs are dyed by rhodamine B (RhB, red), and pressed them into stretched rat skin tissues. The skin is embedded and frozen in an O.C.T. compound, and cut into 10 μm thickness sections for histological observation and drug diffusion analysis. Fig. 3e shows the hematoxylin-eosin (H&E) stained histological section with skin penetrating depth of ~400 μm. In addition, the loaded RhB in MNs can be successfully diffused into tissue confirmed by CLSM after piercing the skin. After 30 min of insertion, RhB can be diffused into the deeper skin tissue (Fig. 3f and 3g).

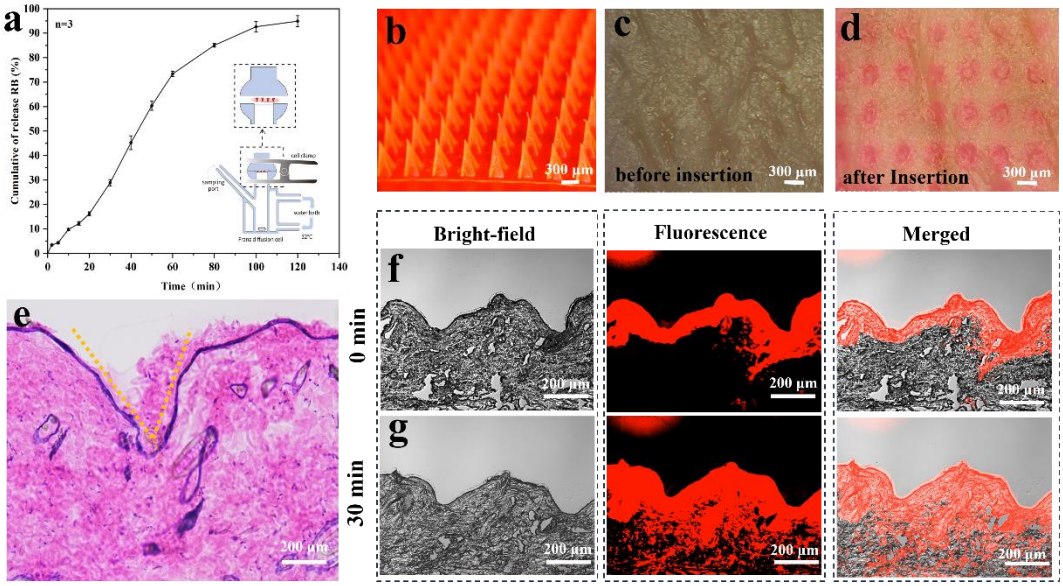

Fig. 3 (a) *In vitro* permeation profile of RB from RB-loaded MNs in PBS (pH 7.4) at 37°C. (b)

Bright-field microscopic images of rhodamine B-laden MNs (c), Rhodamine B-laden MNs before (d) and after piercing the pig skin. (e) H&E-stained histological section image of rat skin after the removal of MN vitro. (f and g) Fluorescent images of RhB-MNs insertion into skin tissue for 0 and 30 min.

3.3 Pharmacodynamic study of RB-loaded MNs

The rat acute migraine models, characterized by ear redness, head-scratching, increased cage climbing, and restlessness, are successfully established by injection of NTG. NTG acts intracellularly through the formation of nitric oxide, which is released from endothelial cells causing vasodilation leading to migraine. Five groups of rats are treated by different treatments after the injection of 2 h. Behavioral changed of head scratching and cage climbing are recorded using 30 min as a statistical period.

Fig. 4a and Table S2 show the changes of head scratching times in different statistic cycles (0-30, 30-60, 60-90, 90-120, 120-180 and 180-240 min). No significant change of head scratching (~30 times/30 min) for the control group can be observed in the whole test procedure. In contrast, the number of head scratching is rapidly increased (~145 times/30 min) in the 1st statistic cycle. Without any treatment, the number of head scratching still can be maintained a higher level (~92 times/30 min) after 4 h. Oral drug is a commonly used treatment method in clinical practice. In the first statistic cycle after oral administration, the number of head scratching can be decreased to ~129 times/30 min compared with ~145 times/30 min for the group without any treatment. And it is gradually decreases to ~66 times/30 min with further extending treatment time to 4 h, exhibiting a certain degree of therapeutic effect. However, in the cases of S.C. and MNs groups, there is a significant decrease of the number of head scratching. In the first 30 min after administration, the numbers of head scratching are ~119 and 121 times/30

min for the S.C. and MNs groups, respectively, showing a slightly lower number than the oral group. Interestingly, the number of head scratching is significantly decreased with extending treatment time due to reducing drug loss and shortening the circulation cycle of drug into the body. And it will be reached ~39 and 38 times/30 min in the 6^{th} statistic cycle, about one-third of the control group and half of oral group. The MNs group exhibits a fast and efficient treatment effect similar to the S.C. group.

Changed of cage climbing times is another behavioral indicator for acute migraine. Fig. 4b and Table S3 show the changes of cage climbing times in different statistic cycles. The cage climbing times are always maintained at a high level state (~27 times/30 min) compared with ~3.5 times/30 min for the control group. After oral administration, the number of cage climbing will be decreased ~19 times/30 min in the first statistic cycle. And it will be further fell back to ~11 times/30 min after 4 h, showing a certain degree of therapeutic effect that is consistent with the changes of head scratching. However, in the cases of S.C. and MNs groups, it will be reached ~15 and 16.5 times/30 min, and further decreasing to ~3.5 and 4.5 times/30 min after 4 h administration.

To investigate the pharmacokinetics of RB delivered by MNs, blood samples are extracted at different time intervals. And the RB concentration in plasma is determined by HPLC. Fig. 4c shows *in vivo* plasma pharmacokinetic profiles of rats with different drug delivery methods using the same dosage of medication (0.5 mg/pcs). The pharmacokinetic profile of RB delivered by MNs is similar to that of S.C. injection. It will reach the peak plasma concentration (C_{max}) of RB at about 60 and 90 min (t_{max}).

The C_{max} for the MNs group is 65.38 ng/mL which is close to 69.24 ng/mL for S.C. injection, and significantly higher than that of oral administration due to the lower bioavailability of RB through the gastrointestinal tract. In addition, the $AUC_{0\text{-}4h}$ for MNs is also close to S.C. group, and far higher than that of oral group (Table S4). These results indicate that MNs delivery can effectively reduce the loss and improve bioavailability of RB. Moreover, the t_{max} for MNs group is higher than that of S.C. group. It may be contributed to swelling and biodegradation of matrix of MNs, leading to delay the intake of drug.

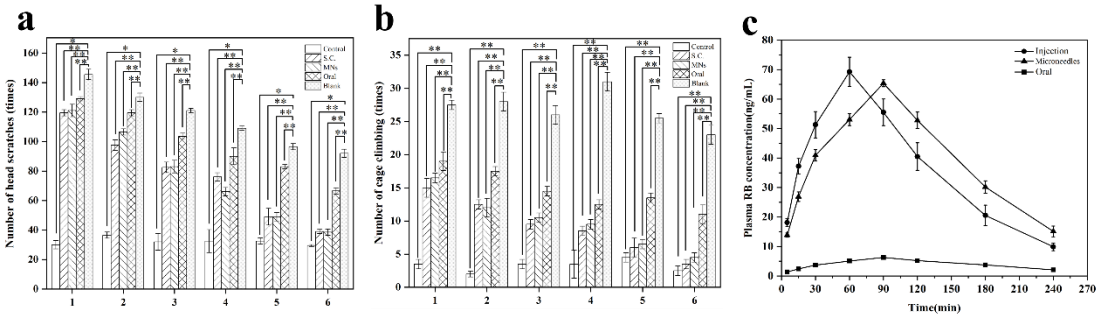

Fig. 4 Behavioral changes in rats with nitroglycerine migraine after administration and changes in blood concentration after administration. (a) Changes of head scratching times in different time periods of rats with different administration methods and the control group, and (b) Changes of cage climbing times in different time periods of rats with different administration methods and the control group. (**p<0.001, compared with the blank group. *p<0.05, compared with the blank group.) (c) *In vivo* plasma pharmacokinetic profiles of rats with different drug delivery methods.

3.4. Immunohistochemical and histopathological tests

Enzyme-linked immunosorbent assay is used to measure the plasma levels of 5-HT, CGRP, and SP, which are key neuropeptides involved in migraine pathophysiology. Fig. 5a shows the levels of 5-HT for the different groups after 2 and 4 h treatment. Table S5 shows the 5-HT levels in plasma at different time intervals for test groups. There's almost nothing changed for the control group at different time intervals. In the case of blank group, the 5-HT levels are 163.52±5.10 and 173.85±3.57 ng/mL which

are lower than the control group due to the secretion inhibition of 5-HT after injection of NTG. The 5-HT levels will be increased slightly after oral drug. They are 172.00±5.95 and 180.33±3.90 ng/mL after 2 and 4 h treatment. However, there will be more upturned in the levels of 5-HT in the cases of S.C. and MNs groups, reaching 182.22±2.99 and 191.22±2.64 ng/mL for S.C. group and 182.26±2.05 and 187.26± 4.63 ng/mL for MNs group after treatment. Fig. 5b and 5c show the levels of CGRP and SP for the different groups after treatment. In the case of control group, the levels of CGRP and SP can be maintained at a relatively lower level. While, the levels of CGRP and SP can be significantly improved in the blank group. And the secretion levels of CGRP and SP will be inhibited in the oral group, showing a certain degree of therapeutic effect. However, the levels of CGRP and SP can be effectively inhibited in the S.C. and MNs groups (Table S6 and S7). These results indicated that MNs therapy had a similar therapeutic effect as S.C. therapy and was significantly superior to oral treatment.

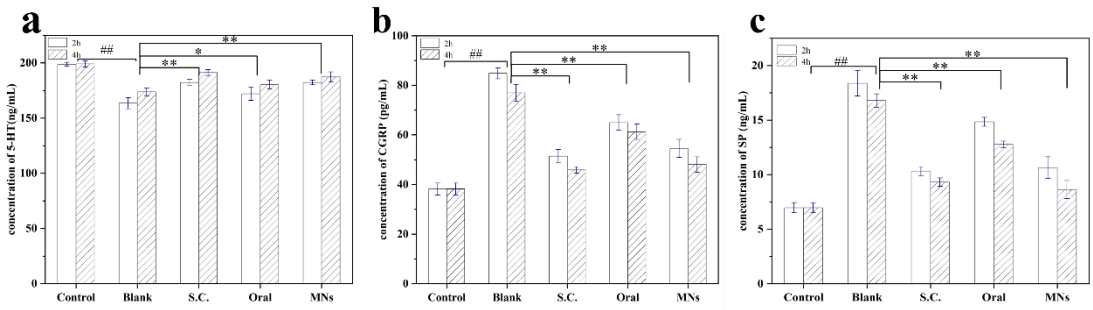

Fig. 5 Changes in relevant neurotrophic factors after treatment with different routes of administration. (a) The 5-HT ELISA kit was used to detect the plasma 5-HT level in different administration modes and control groups, (b) The CGRP ELISA kit was used to detect the plasma CGRP level in different administration modes and control groups, (c) The SP ELISA kit was used to detect the plasma SP level in different administration modes and control groups. (##$p<0.001$, compared with control administration. **$p<0.001$, compared with the blank group. *$p<0.05$, compared with the blank group.)

3.5. Analysis of paraffin sections of rat brainstem portions

Fig. 6a-e show the immunohistochemical images of brainstem sections from different groups of rats. NTG-activated c-Fos immunoreactive neurons and negative cells are shown in brownish yellow and bluish violet, respectively. More number of brown-yellow clumps in blank group can be observed compared with that in the control group. However, the brown-yellow positive expression in the oral group is lower than that in the blank group. In contrast, the MNs group and the S.C. group significantly are down-regulated the expression of c-Fos positive cells. Fig. 6f and Table S8 show the results of c-fos expression in the immunohistochemistry and the quantification of these c-fos-positive cells. The control group show a small number of c-fos-positive cells (4.87±1.36) and the blank group present the highest number of c-fos-positive cells (24.24±4.32). After oral treatment, the number of c-fos-positive cells can be decreased to 16.77±2.84, showing a certain degree of decrease compared to the blank group. However, in the cases of S.C. and MNs groups, the number of c-fos-positive cells are 9.43±4.29 and 12.11±3.66, respectively. Based on the above results, MNs drug delivery is a potential candidate for migraine treatment via up-regulating the level of 5-HT and down-regulating the levels of CGRP and SP, and inhibiting c-fos-positive cells expression.

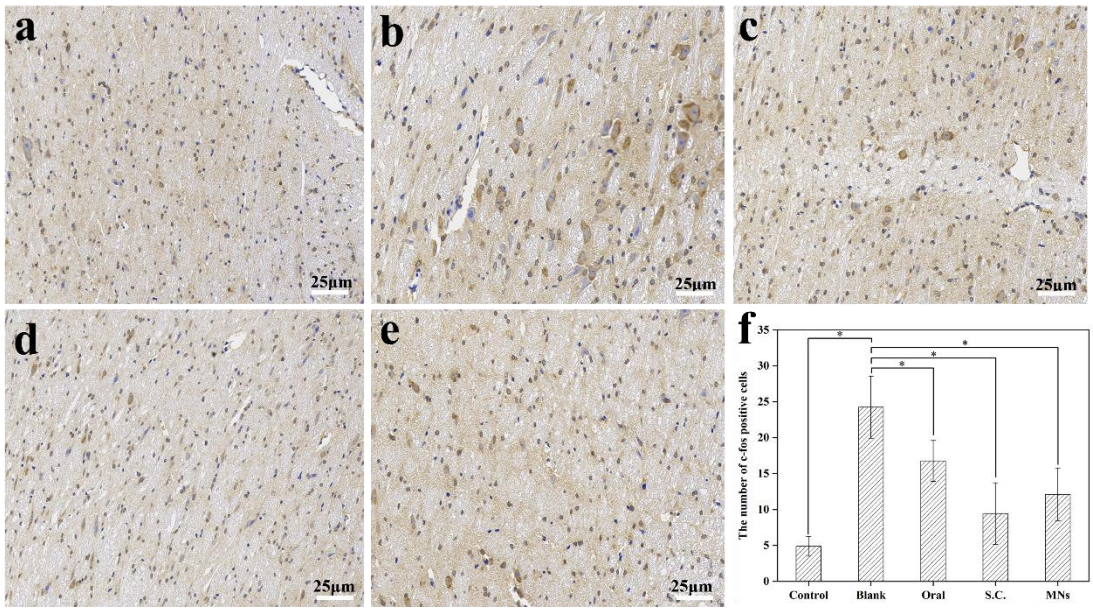

Fig. 6 Tissue slice images of the brain stem in each group of rats. (a) control, (b) blank, (c) oral, (d) S.C. and (e) MNs groups, and (f) Statistical plot of the number of c-fos positive cells (*$p<0.05$, compared with the blank group).

4. Conclusion

This study demonstrated that MNs had the advantages of being painless, effective, safe, and were the efficient transdermal route of administration. RB was loaded into MNs to form RB-loaded MNs, which showed a remarkable effect similar to subcutaneous injection for the treatment of acute migraine compared with oral administration. The P(VP-co-VA)/PVA polymer matrix affected the mechanical and insertion properties of MNs, and improved the skin penetration of nanoparticles. The prepared MNs had sufficient mechanical strength to penetrate the skin and form microchannels for transdermal drug delivery. Pharmacodynamic tests showed that the fabricated RB-loaded MNs had the efficacy of reducing head scratching and cage climbing after injection of nitroglycerin. Immunohistochemical analysis and histopathological images supported the safety of RB-loaded MNs. Therefore, the development of non-invasive and fast-dissolving MNs could be a potential option for

effective transdermal treatment of acute migraine, with reduced long-term risks and better patient compliance.

Declaration of Competing Interests

The authors declare that they have no known competing financial interests or personal relationships that could have appeared to influence the work reported in this paper.

Data availability

Data will be fabricated available on request.

Acknowledgments

This research was supported by the Huadong Medicine Joint Funds of the Zhejiang Provincial Natural Science Foundation of China under Grant No. LHDMZ23H300003, Science and Technology Planning Project of Hangzhou Health Commission under Grant No. 20220919Y011, and National Natural Science Foundation of China under Grant No. 51873194.

References

[1] GBD 2017 Disease and Injury Incidence and Prevalence Collaborators, Global, regional, and national incidence, prevalence, and years lived with disability for 354 diseases and injuries for 195 countries and territories, 1990–2017: a systematic analysis for the Global Burden of Disease Study 2017, Lancet, 392 (2018) 1789–1858.

[2] American Headache Society, The American Headache Society position statement

on integrating new migraine treatments into clinical practice, Headache, 59 (2019) 1–18.

[3] Cenk Ayata, Cortical spreading depression triggers migraine attack: pro, Headache, 50 (2010) 725–730.

[4] Peer Tfelt-Hansen, Pharmacological strategies to treat attacks of episodic migraine in adults, Expert Opin. Pharmacother., 22 (2021) 305–316.

[5] Pablo Ávalos Prado, Arnaud Landra-Willm, Clément Verkest, Aurore Ribera, Anne-Amandine Chassot, Anne Baron, Guillaume Sandoz, TREK channel activation suppresses migraine pain phenotype, iScience, 24 (2021) 102961.

[6] Minoti Bhakta, Trang Vuong, Tetsuya Taura, David S Wilson, Jennifer R Stratton, Kimberly D Mackenzie, Migraine therapeutics differentially modulate the CGRP pathway, Cephalalgia, 41 (2021) 499–514.

[7] Kristian Agmund Haanes, Lars Edvinsson, Pathophysiological mechanisms in migraine and the identification of new therapeutic targets, CNS Drugs, 33 (2019) 525–537.

[8] Yavuz Yücel, Salih Coşkun, Beyhan Cengiz, Hasan H. Özdemir,1 Ertuğrul Uzar, Abdullah Çim, M. Akif Camkurt, M. Ufuk Aluclu1, Association of polymorphisms within the serotonin receptor genes 5-HT_{R1A}, 5-HT_{R1B}, 5-HT_{R2A} and 5-HT_{R2C} and migraine susceptibility in a turkish population, Clin. Psychopharm. Neu., 14 (2016) 250–255.

[9] Carlos M Villalón, Antoinette Maassen VanDenBrink, The role of 5-hydroxytryptamine in the pathophysiology of migraine and its relevance to the

design of novel treatments, Mini. Rev. Med. Chem., 17 (2017) 928–938.

[10] Liping Fang, Shan He, Peng Yin, Ning Wang, Bin Zhang, Haixiao Jin, Design, synthesis, and structure–Activity relationship studies of novel tryptamine derivatives as 5–HT_{1B} receptor agonists, J. Mol. Struct., 1265 (2022) 133320.

[11] M D Ferrari, P J Goadsby, K I Roon, R B Lipton, Triptans (serotonin, 5-$HT_{1B/1D}$ agonists) in migraine: detailed results and methods of a meta-analysis of 53 trials, Cephalalgia, 22 (2002) 633–658.

[12] Silvia Benemei, Francesca Cortese, Alejandro Labastida-Ramírez, Francesca Marchese, Lanfranco Pellesi, Michele Romoli, Anne Luise Vollesen, Christian Lampl, Messoud Ashina, School of Advanced Studies of the European Headache Federation (EHF-SAS), Triptans and CGRP blockade-impact on the cranial vasculature, J. Headache Pain, 18 (2017) 103.

[13] Rashid Giniatullin, 5-hydroxytryptamine in migraine: the puzzling role of ionotropic 5-HT_3 receptor in the context of established therapeutic effect of metabotropic 5-HT_1 subtypes, Br. J. Pharmacol., 179 (2022) 400–415.

[14] Paul G Mathew, Brad C Klein, Getting to the heart of the mater: migraine, triptans, DHE, ditans, CGRP antibodies, first/second-generation gepants, and cardiovascular risk, Headache, 59 (2019) 1421–1426.

[15] Miguel J A Láinez, Rizatriptan in the treatment of migraine, Neuropsych. Dis. Treat., 2 (2006) 247–259.

[16] Pin-Chung Huang, Fu-Chi Yang, Ching-Mao Chang, Chun-Pai Yang, Targeting the 5-$HT_{1B/1D}$ and 5-HT_{1F} receptors for acute migraine treatment, Prog. Brain Res.,

255 (2020) 99–121.

[17] Brenden Cheong-Qi Seah, Boon Mian Teo. Recent advances in ultrasound-based transdermal drug delivery, Int. J. Nanomedicine., 13 (2018) 7749–7763.

[18] J H Gaddum, The stability of watery solutions of the oxytocic principle of the pituitary gland, Biochem. J., 24 (1930) 939–944.

[19] Roshni Ramachandran, Neurogenic inflammation and its role in migraine, Semin. Immunopathol., 40 (2018) 301–314.

[20] M Carballo-Quintás, I Martínez-Silva, C Cadarso-Suárez, M Alvarez-Figueiras, F J Ares-Pena, E López-MartínA, study of neurotoxic biomarkers, c-fos and GFAP after acute exposure to GSM radiation at 900 MHz in the picrotoxin model of rat brains, Neurotoxicology., 32 (2011) 478-94.

[21] Zsuzsanna Bohár, Annamária Fejes-Szabó, Lilla Tar, Hedvig Varga, János Tajti, Árpád Párdutz, László Vécsei, Evaluation of c-Fos immunoreactivity in the rat brainstem nuclei relevant in migraine pathogenesis after electrical stimulation of the trigeminal ganglion, Neurol. Sci., 34 (2013) 1597-604.

[22] Cetinkaya, A., Kilinc, E., Camsari, C., & Ogun, M. N., Effects of estrogen and progesterone on the neurogenic inflammatory neuropeptides: Implications for gender differences in migraine, Exp. Brain Res., 238 (2020), 2625–2639.

[23] Rashid Giniatullin, 5-hydroxytryptamine in migraine: the puzzling role of ionotropic 5-HT3 receptor in the context of established therapeutic effect of metabotropic 5-HT1 subtypes, Br. J. Pharmacol., 179 (2022) 400–415.

[24] R V Keny 1, Chrisma Desouza, C F Lourenco, Formulation development and

evaluation of orally disintegrating tablets rizatriptan benzoate, Indian J. Pharm. Sci., 72 (2010) 79-85.

[25] Kassem, Abeer Ahmed, formulation approaches of triptans for management of migraine, curr. drug deiv., 13 (2016) 882-898.

[26] Ashish Chokshi, Ravi Vaishya, Rachana Inavolu, Formulation and evaluation of rizatriptan benzoate mouth disintegrating tablets, Int. J. Pharm., 571 (2019) 118702.

[27] Per G Djupesland, John C Messina, Ramy A Mahmoud, The nasal approach to delivering treatment for brain diseases: an anatomic, physiologic, and delivery technology overview, Ther. Deliv., 5 (2014) 709-733.

[28] Priti Girotra, Shailendra Kumar Singh, Multivariate optimization of rizatriptan benzoate-loaded solid lipid nanoparticles for brain targeting and migraine management, AAPS PharmSciTech., 18 (2017) 517-528.

[29] Brenden Cheong-Qi Seah, Boon Mian Teo, Recent advances in ultrasound-based transdermal drug delivery, Int. J. Nanomedicine, 13 (2018) 7749–7763.

[30] Kevin Ita, Recent progress in transdermal sonophoresis, Pharm. Dev. Technol ., 22 (2017) 247–259.

[31] Liming Ruan, Gao Song, Xueya Zhang, Tianqi Liu, Yanfang Sun, Junlan Zhu, Zhiyong Zeng, Guohua Jiang, Transdermal delivery of multifunctional CaO_2@Mn-PDA nanoformulations by microneedles for NIR-induced synergistic therapy against skin melanoma, Biomater. Sci., 9 (2021) 6830-6841.

[32] Tejashree Waghule, Gautam Singhvi, Sunil Kumar Dubey, Murali Monohar

Pandey, Gaurav Gupta, Mahaveer Singh, Kamal Dua, Microneedles: a smart approach and increasing potential for transdermal drug delivery system, Biomed. Pharmacother., 109 (2019) 1249–1258.

[33] Dan Wu, Yingshu Quan, Fumio Kamiyama, Kosuke Kusamori, Hidemasa Katsumi, Toshiyasu Sakane, Akira Yamamoto, Improvement of transdermal delivery of sumatriptan succinate using a novel self-dissolving microneedles array fabricated from sodium hyaluronate in rats, Biol. Pharm. Bull., 38 (2015) 365–373.

[34] Buchi N Nalluri, Sai Sri V Anusha, Sri R Bramhini, J Amulya, Ashraf S K Sultana, Chandra U Teja, Diganta B Das, In vitro skin permeation enhancement of sumatriptan by microneedles application, Curr. Drug. Deliv., 12 (2015) 761–769.

[35] Ipshita Menon, Priyal Bagwe, Keegan Braz Gomes, Lotika Bajaj, Rikhav Gala, Mohammad N Uddin, Martin J D'Souza, Susu M Zughaier, Microneedles: a new generation vaccine delivery system, Micromachines, 12 (2021) 435.

[36] Ragini Amarnani, Pravin Shende, Microneedles in diagnostic, treatment and theranostics: An advancement in minimally-invasive delivery system, Biomed. Microdevices, 4 (2022) 24.

[37] Sumin Han, Panjae Lee, Hyo-Jick Choi, Non-invasive vaccines: challenges in formulation and vaccine adjuvants, Pharmaceutics, 15 (2023) 2114.

[38] Zhaowenbin Zhang, Wenbo Li, Di Chang, Ziqin Wei, Endian Wang, Jing Yu, Yuze Xu, Yumei Que, Yanxin Chen, Chen Fan, Bing Ma, Yanling Zhou, Zhiguang Huan, Chen Yang, Feng Guo, Jiang Chang, A combination therapy for androgenic alopecia based on quercetin and zinc/copper dual-doped mesoporous silica

nanocomposite microneedle patch, Bioact. Mater., 24 (2022) 81-95.

[39] Andi Dian Permana, Firzan Nainu, Kurtis Moffatt, Eneko Larrañeta, Ryan F Donnelly, Recent advances in combination of microneedles and nanomedicines for lymphatic targeted drug delivery, Wires. Nanomed. Nanobi., 13 (2021) e1690.

[40] Dan Wu, Hidemasa Katsumi, YingShu Quan, Fumio Kamiyama, Kosuke Kusamori, Toshiyasu Sakane, Akira Yamamoto, Permeation of sumatriptan succinate across human skin using multiple types of self-dissolving microneedle arrays fabricated from sodium hyaluronate, J. Drug Target, 24 (2016) 752–758.

[41] Sean P Sullivan, Dimitrios G Koutsonanos, Maria Del Pilar Martin, Jeong Woo Lee, Vladimir Zarnitsyn, Seong-O Choi, Niren Murthy, Richard W Compans, Ioanna Skountzou, Mark R Prausnitz, Dissolving polymer microneedle patches for influenza vaccination, Nat. Med., 16 (2010) 915–920.

[42] Jae Hwan Jung, Sung Giu Jin, Microneedle for transdermal drug delivery: current trends and fabrication, J. Pharm. Investig., 4 (2021) 503-517.

[43] Jian Chen, Hui Ren, Pan Zhou, Shuai Zheng, Bin Du, Xiaowen Liu, Fei Xiao, Microneedle-mediated drug delivery for cutaneous diseases, Front. Bioeng. Biotechnol., 10 (2022) 1032041.

[44] H R Kavya, S Bhattacharyya, Statistical optimization and evaluation of a multi release unit bilayer tablet of rizatriptan benzoate, Indian J. Pharm. Sci., 83 (2021) 52-59.

[45] Na Xu, Manyue Zhang, Wenxin Xu, Guixia Ling, Jia Yu, Peng Zhang, Swellable PVA/PVP hydrogel microneedle patches for the extraction of interstitial skin fluid

toward minimally invasive monitoring of blood glucose level, Analyst, 147 (2022) 1478-1491.

[46] Hojatollah Rezaei Nejad, Aydin Sadeqi, Gita Kiaee, Sameer Sonkusale, Low-cost and cleanroom-free fabrication of microneedles, Microsyst. Nanoeng., 15 (2018) 17073.

[47] Disha Shetty, Dani Lakshman Yarlagadda, Bheemisetty Brahmam, Swapnil J. Dengale, Shaila A. Lewis, Investigating the influence of the type of polymer on sustaining the supersaturation from amorphous solid dispersions of Apremilast and its pharmacokinetics, J. Drug Deliv. Sci. Technol., 84 (2023) 104520.

[48] Hiep X Nguyen, Chien N Nguyen, Microneedle-mediated transdermal delivery of biopharmaceuticals, Pharmaceutics, 15 (2023) 277.

[49] Malte Bille Rask, Matthias Manne Knopp, Niels Erik Olesen, René Holm, Thomas Rades. Influence of PVP/VA copolymer composition on drug–polymer solubility. Eur. J. Pharm. Sci., 85 (2016) 10–17.

[50] Loriane Moreira Martins, Gabriel Nardi Fraga, Michelly Cristina Galdioli Pellá, Felipe Augusto Chimenez Pinto, Francielly de Souza, Jean Colombari Neto, Ariane Regina Souza Rossin, Josiane Caetano, Douglas Cardoso Dragunski, Poly(1-vinylpyrrolidone-co-vinyl-acetate)-based electrospun dissolvable nanofibrous film for quercetin administration, Process Biochem., 122 (2022) 8–15.

[51] Ting Liu, Minglong Chen, Jintao Fu, Ying Sun, Chao Lu, Guilan Quan, Xin Pan, Chuanbin Wu, Recent advances in microneedles-mediated transdermal delivery of Protein and peptide drugs, Acta Pharm. Sin. B, 11 (2021) 2326–2346.

[52] Jordan A Stinson, Archana V Boopathy, Brian M Cieslewicz, Yichen Zhang, Nickolas W Hartman, David P Miller, Matthew Dirckx, Brett L Hurst, E Bart Tarbet, Jonathan A Kluge, Kathryn M Kosuda, Enhancing influenza vaccine immunogenicity and efficacy through infection mimicry using silk microneedles, Vaccine, 39 (2021) 5410–5421.

[53] Lin Niu, Leonard Y Chu, Scott A Burton, Jayanth Panyam, Intradermal delivery of vaccine nanoparticles using hollow microneedle array generates enhanced and balanced immune response, J. Control Release, 294 (2019) 268–278.

[54] Ke Peng, Lalitkumar K Vora, Ismaiel A Tekko, Andi Dian Permana, Juan Domínguez-Robles, Delly Ramadon, Philip Chambers, Helen O McCarthy, Eneko Larrañeta, Ryan F Donnelly, Dissolving microneedle patches loaded with amphotericin B microparticles for localised and sustained intradermal delivery: potential for enhanced treatment of cutaneous fungal infections, J. Control. Release, 339 (2021) 361–380.

[55] Hiep X Nguyen, Behnam Dasht Bozorg, Yujin Kim 1, Alena Wieber, Gudrun Birk, Dieter Lubda, Ajay K Banga, Poly (vinyl alcohol) microneedles: fabrication, characterization, and application for transdermal drug delivery of doxorubicin, Eur. J. Pharm. Biopharm., 129 (2018) 88–103.

[56] Jes Olesen, Inger Jansen-Olesen, Towards a reliable animal model of migraine, Cephalalgia, 32 (2012) 570–580.

[57] Rui-Hai Zhou, William H Frishman, The antiplatelet effects of nitrates: is it of clinical significance in patients with cardiovascular disease, Cardiol. Rev., 18

(2010) 129–135.

[58] Mengyuan Hou, Hongxia Liu, Yunfei Li, Ling Xu, Yingchun He, Yinghua Lv, Qingshan Zheng, Lujin Li, Efficacy of triptans for the treatment of acute migraines: a quantitative comparison based on the dose-effect and time-course characteristics, Eur. J. Clin. Pharmacol., 24 (2019) 1369-1378.

[59] R. Manjuladevi, M. Thamilselvan, S. Selvasekarapandian, R. Mangalam, M. Premalatha, S. Monisha, Mg-ion conducting blend polymer electrolyte based on poly(vinyl alcohol)-poly (acrylonitrile) with magnesium perchlorate, Solid State Ion., 308 (2017) 90-100.

[60] S. Y. Poy, S. Bashir, F. S. Omar, N. M. Saidi, N. K. Farhana, V. Sundararajan, K. Ramesh, S. Ramesh, Poly (1-vinylpyrrolidone-co-vinyl acetate) (PVP-co-VA) based gel polymer electrolytes for electric double layer capacitors (EDLC), J. Polym. Res., 27 (2020) 50-60.

[61] Leonard Ionut Atanase, Sophie Bistaca, Gérard Riess, Effect of poly(vinyl alcohol-co-vinyl acetate) copolymer blockiness on the dynamic interfacial tension and dilational viscoelasticity of polymer–anionic surfactant complex at the water–1-chlorobutane interface, Soft Matter, 11 (2015) 2665-2672.